PROCEEDINGS OF SCIENCE

Long-term calibration and stability of the Auger Engineering Radio Array using the diffuse Galactic radio emission

R. M. de Almeida[a,*] **for the Pierre Auger Collaboration**[b]

[a] *Universidade Federal Fluminense,*
Av. dos Trabalhadores 424, Volta Redonda, Brazil
[b] *Observatorio Pierre Auger, Av. San Martín Norte 304, 5613 Malargüe, Argentina*
Full author list: https://www.auger.org/archive/authors_icrc_2023.html

E-mail: spokespersons@auger.org

The Auger Engineering Radio Array (AERA), part of the Pierre Auger Observatory, is currently the largest facility to measure radio emissions from ultra-high energy extensive air showers. It comprises 153 autonomous radio-detector stations, covering an area of 17 km^2, and measures radio waves in the frequency range from 30 to 80 MHz. An accurate description of the detector response is necessary to interpret the data collected by the stations correctly. Previously, this was achieved by measuring the analog chain in the laboratory and simulating and measuring the directional response of the antenna. In this work, we perform an absolute calibration using the continuously monitored sidereal modulation of the diffuse Galactic radio emission. The calibration is performed by comparing the average spectra recorded by the stations with a model of the full radio sky propagated through the system response, including the antenna, filters, and amplifiers. We describe the method to determine the calibration constants for each antenna and present the corresponding results. Furthermore, the behavior of the calibration constants is studied as a function of time. There is no relevant aging effect over a timescale of a decade, which shows that radio detectors could help monitor possible aging effects of other detector systems during long-term operations, stressing their importance in determining an absolute energy scale.

38th International Cosmic Ray Conference (ICRC2023)
26 July - 3 August, 2023
Nagoya, Japan

ICRC2023
38th International Cosmic Ray Conference
The Astroparticle Physics Conference

*Speaker

PoS(ICRC2023)279

1. Introduction

The Auger Engineering Radio Array (AERA)[1] is currently the largest system designed to measure radio emissions from ultra-high energy extensive air showers. It operates within the frequency range of 30 – 80 MHz and utilizes two channels, each one measuring in a different polarization: East-West and North-South relative to magnetic North. A precise characterization of the detector's response is crucial for the accurate interpretation of the data collected by the stations. In the past, this was accomplished by conducting measurements on the analog chain in the laboratory, as well as simulating and measuring the directional response of the antennas. In this study, we adopt a different approach by performing an absolute Galactic calibration of the AERA antennas. Calibration constants are obtained by comparing the average spectra recorded by the stations with a comprehensive model of the entire radio sky propagated through the system response taking into account the antenna, filters, and amplifiers. Additionally, we study the behavior of the calibration constants over time from 2014 until 2020.

The proceeding is structured as follows: Section 2 presents the data set utilized for the calibration process. Section 3 describes the radio sky model employed in this study, while Section 4 presents a comprehensive explanation of the methodology adopted for the absolute Galactic calibration as well as the results. The investigation of calibration constants over time is discussed in Section 5. Finally, Section 6 summarizes the conclusions drawn from the study.

2. Data set

Since AERA is an engineering array, various antenna types, electronics, and trigger systems have been developed, deployed, and tested in the field over time. The deployment was done in three phases, and the distribution of the electronics over the antenna stations changed multiple times. In this study, we use data measured by Butterfly antennas and Logarithmic-Periodic Dipole Antennas (LPDA)[1] that can handle external triggers provided by the baseline Auger detectors. The absolute Galactic calibration is performed by using periodically triggered traces measured with 52 Butterfly antennas from 2014 until 2020, 23 Butterfly antennas with data collected from January 2016 until 2020, and 14 LPDA antennas with available data from 2017 to 2020.

Periodically triggered traces refer to the read-out requests made by each data acquisition system for all active stations every 100 seconds. The traces are corrected for an observed anti-correlation between peak amplitude and temperature caused by temperature-dependent gain variations of amplifiers in the signal chain, which had been characterized previously in lab measurements. The time series of each trace is clipped to 1024 samples (5.7μs), which corresponds to 285 frequency bins, with a width of $\Delta\nu = 0.175$ MHz, within the range of 30 – 80 MHz. For Galactic calibration purposes, we compute the power within each frequency band ν, which has a width of $\delta\nu = 1$ MHz, by using

$$P_\nu = \frac{2}{T} \sum_{k=\nu-\delta\nu/2}^{\nu+\delta\nu/2} \frac{|V(k)|^2}{Z_L} \Delta\nu, \tag{1}$$

where T is the length of the trace, $V(k)$ is the measured spectral voltage at frequency k and $Z_L = 50\ \Omega$ is the antenna impedance. The factor of 2 arises from utilizing only half of the FFT

spectra. Since all stations are located in approximately the same geographic region, the variation of the Galactic signal is the same for all antennas. Nevertheless, the background signal measurement encompasses a combination of the Galactic component and various other types of noise. The intensity of these noise components can vary depending on the source of the signal. Therefore, it is essential to preprocess the data by reducing these noise components before proceeding with the Galactic calibration.

2.1 Data cleaning

A Galactic modulation of the radio intensity as a function of Local Sidereal Time (LST) results from the passage of the Galaxy across the Auger site and can be observed by using periodic data. However, the periodic traces also contain cosmic ray signals, radio frequency interference (RFI) from external sources, and internal electronic noise. RFIs can be classified into two categories: broadband and narrowband. Narrowband noise is characterized by continuous emissions throughout the entire LST range caused by sources that emit persistently radio signals at specific frequencies. The most intense narrowband noises observed in the AERA periodically triggered traces are produced by the beacons installed at the Auger site for time calibration purposes. The amplitude of these noises makes it difficult to detect the passage of the Galaxy in the dynamic frequency spectrum. Thus, these frequency bands are identified and removed from the data set with the corresponding gaps linearly interpolated. As an illustration, Fig.1 presents the dynamic average frequency spectrum obtained for a specific antenna. The left panel shows the spectrum before the RFI subtraction for the East-West channel, while the right panel shows the spectrum after the RFI subtraction. It can be observed that the Galactic modulation becomes evident once the noise is eliminated.

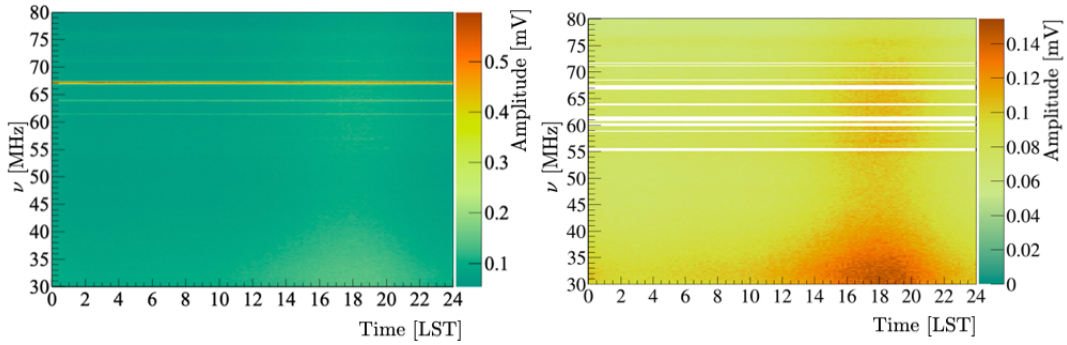

Figure 1: Dynamic average frequency spectrum as a function of LST for the East-West channel of antenna Butterfly-KIT/BUW ID:53 considering the period of February 2017. The left panel presents the results before removal of narrowband RFI (horizontal lines) while the right one shows that the Galactic signal modulation becomes evident after RFI removal.

On the other hand, broadband RFIs manifest as transient radio pulses and can also contaminate the data. To mitigate the effects of broadband noise and cosmic ray signals, a threshold as a function of LST to reject/accept traces is implemented for each station. First, we compute the average spectral density of each trace according to

$$I = \frac{1}{N}\sqrt{\sum_{i=1}^{N} A^2(\nu_i)}, \tag{2}$$

where $A(\nu_i)$ is the signal amplitude in frequency bin i and N is the total number of frequency bins. For each 20-minute bin in LST, a Gaussian fit is performed on the distribution of I values, and a threshold $I^{\rm th}_{\rm LST}$ corresponding to 3σ is obtained by solving $\int_{-\infty}^{I^{\rm th}_{\rm LST}} G(I;\bar{I},\sigma_I) = 0.9973$, where $\bar{I}$ and σ_I are the average and RMS of the Gaussian distribution, respectively. The threshold $I^{\rm th}_{\rm LST}$ is computed for each channel on a monthly basis. Traces with average spectral densities I greater than $I^{\rm th}_{\rm LST}$ are removed from the data.

3. Radio sky model

The background radio signal received at Earth varies in different directions across the sky and can be conveniently specified by its equivalent brightness temperature. In this way, radio maps of the sky are produced by using measured brightness temperature. For the frequency range of the AERA stations (30 − 80 MHz), the background signal is dominated by Galactic emission, and the total expected power to be received by the antenna is calculated as

$$P_{\rm sky}(t,\nu) = \frac{Z_0}{Z_{\rm L}}\frac{k_{\rm B}}{c^2}\int_{\Omega} \nu^2 T_{\rm sky}(\nu,\alpha,\delta)|H_e(\nu,\alpha,\delta)|^2 d\Omega, \tag{3}$$

where $k_{\rm B}$ is the Boltzmann constant, c is the speed of light, Z_0 is the impedance of free space given by $120\pi\Omega$, and $Z_{\rm L}$ is the antenna impedance. $H_e(\nu,\alpha,\delta)$ is the Vector Effective Length (VEL) that is represented by a 2-dimensional vector with complex entries and gives the directional response of the antenna at a given frequency ν as a function of the right ascension α and declination δ. $T_{\rm sky}(\nu,\alpha,\delta)$ is the temperature of the sky at a given frequency ν and direction (α,δ) obtained from radio sky models, described as a combination of the cosmic microwave background (CMB), an isotropic emission due to extragalactic sources unresolved and an anisotropic Galactic emission. There are different available models for the sky radio emission as LFmap[2], GSM 2008[3], GSM 2016[3], LFSM[4], GMOSS[5], SSM[6] and ULSA[7]. In this work, the LFmap model is utilized as it provides a close representation of the average model. An estimate of the systematic uncertainties on the prediction of the Galactic emission from sky models was obtained in [8]. Figure 2 shows the expected power $P_{\rm sky}(t,\nu)$ to be received from the sky as a function of LST and frequency by considering the LFmap model and the directional response of Butterfly and LPDA antennas for the East-West channel.

4. Calibration Method and Results

For a correct interpretation of AERA data, is necessary an accurate knowledge of the whole signal chain (antenna, amplifiers, filters, and digitizer) in order to reduce measurement uncertainties. Therefore, the antennas must be carefully calibrated. For this, an approach inspired by the calibration technique used in the LOFAR experiment [9] was used. We consider the convolution of the power received from the sky $P_{\rm sky}$ with the gains and noises entering the antenna signal chain, but also take

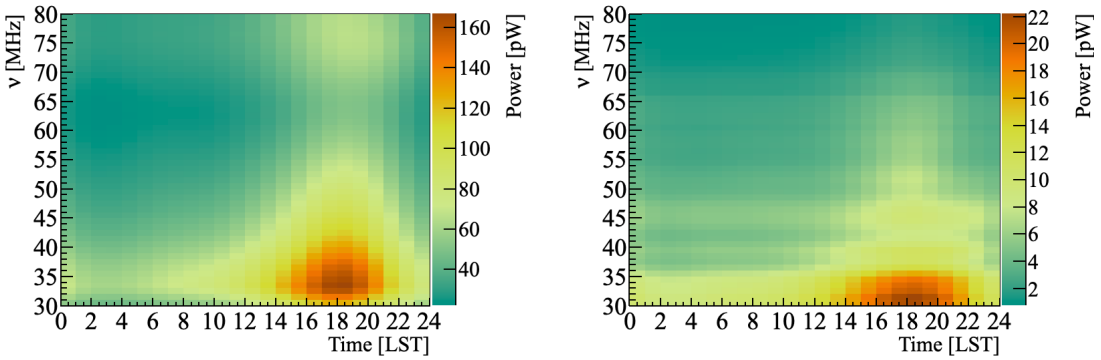

Figure 2: Expected power spectrum to be received from the sky for Butterfly (left) and LPDA (right) antennas in the East-West channel.

into account a possible external environmental noise. This way, the model of the power received from the sky and propagated by the antenna can be described by

$$P_{\text{model}}(t,\nu) = P_{\text{sky}}(t,\nu)G_{\text{ant}}(\nu)G_{\text{RCU}}(\nu)C_0^2(\nu) + N_{\text{tot}}(\nu), \tag{4}$$

in which $G_{\text{ant}}(\nu)$ and $G_{\text{RCU}}(\nu)$ are, respectively, the gains of the Low Noise Amplifier (LNA) and of the Receiver Unit (RCU), where the signal is subjected to a bandpass filter, amplified and digitized. Besides, $C_0(\nu)$ is the calibration constant that needs to be determined and the total noise $N_{\text{tot}}(\nu)$ is a sum of the intrinsic electronic thermal noise and the environmental one. To perform the calibration, we compare the average of measured power at the antenna, described by Eq.1, in bins of LST and frequency, with the expected power, described by Eq.4. Thus, for each frequency band, we conduct a linear regression analysis by fitting the expected power P_{model} against the measured power P_ν. This regression allows us to determine the values of $C_0^2(\nu)$ and $N_{\text{tot}}(\nu)$ associated with each frequency band. As an example, the left panel of Fig.3 illustrates the graph depicting the measured power versus the expected power, along with the resulting linear fits obtained for each frequency band considering the North-South channel of antenna Id: 27. These fits were derived using periodic traces collected during January 2021. The right panels of the same figure show the values of the calibration constants C_0 (top panel) and total noise (bottom panel) obtained from the fit.

The calibration for each channel is performed on a monthly basis. Figure 4 displays the distribution of the average calibration constants obtained for each antenna, denoted as $\langle C_0 \rangle = \langle C_0(\nu) \rangle$. The left and right panels represent the distribution obtained for the East-West (red histograms with hatch patterns) and North-South (solid gray histograms) channels of all Butterfly and LPDA antennas, respectively, throughout the entire analyzed time period. The calibration constants obtained are close to 1 (differing less than 3% for Butterfly antennas and $\sim$ 5% for LPDA stations), indicating a good agreement with the original calibration, performed by measuring the analogue chain in the laboratory and simulating the directional response of the antenna. The observed shift between the North-South and East-West channels in Butterfly antennas is a consequence of imperfect modeling of the electronics box, which has an impact on the directional response of the East-West channel.

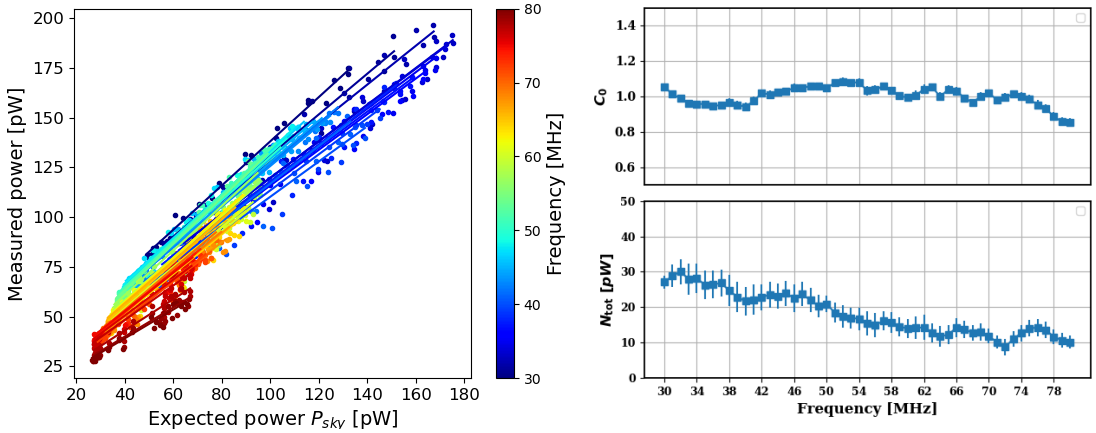

Figure 3: Left panel: graph of the measured power versus the expected power as well as the resulting linear fits obtained for each frequency band with respect to the North-South channel of the Butterfly antenna Id: 27 by using periodic traces collected during January of 2021. Right panels: calibration constants C_0 (top panel) and total noise (bottom panel) obtained from the fit.

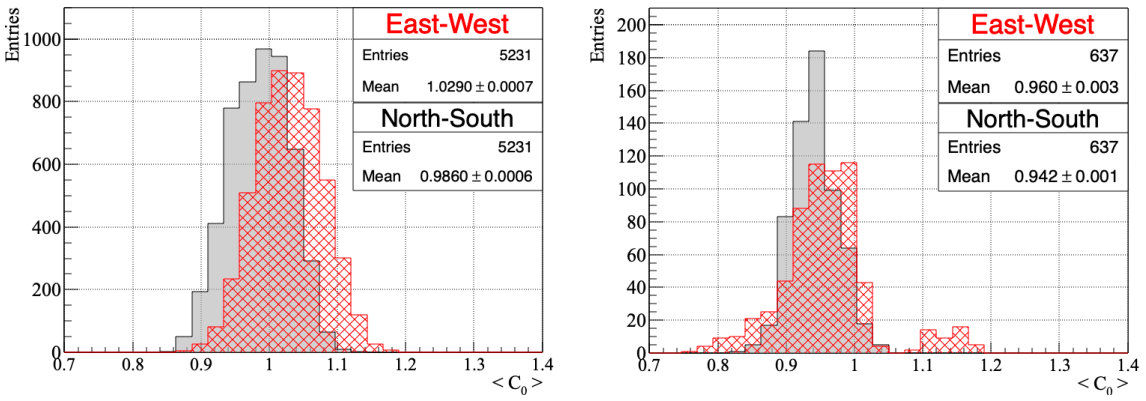

Figure 4: Distribution of the average calibration constants of all Butterfly (left panel) and LPDA (right panel) antennas during the entire period considered. Red and gray histograms correspond to the East-West and North-South channels, respectively.

5. Study of the calibration constants as a function of time

In this section, we study the time behavior of the calibration constants over the whole data-taking period. For this, we consider the evolution of the average of the calibration constants obtained for each frequency, $\langle C_0 \rangle$. As an example, Fig.5 presents the behavior of the calibration constants for both channels of antenna Id:33 from 2014 until the end of 2020. As one can see, even after correcting for the temperature-dependent gain variations of amplifiers in the signal chain, a remaining seasonal modulation with unknown origin is observed. Accounting for this modulation, the time behavior of the calibration constant is parameterized by $< C_0(t') >= A\cos(\frac{\pi}{6}t' + \phi) + at' + b$. The parameters A and ϕ represent the magnitude and phase of the observed seasonal modulation, respectively, around the baseline value b (in the absence of aging). The variable t' denotes the time in months since the start of data taking, and the slope parameter a is of special interest because it is interpreted

in terms of aging of the station per month. The fit of the calibration constants over time shown in Fig.5 is represented by the red curve.

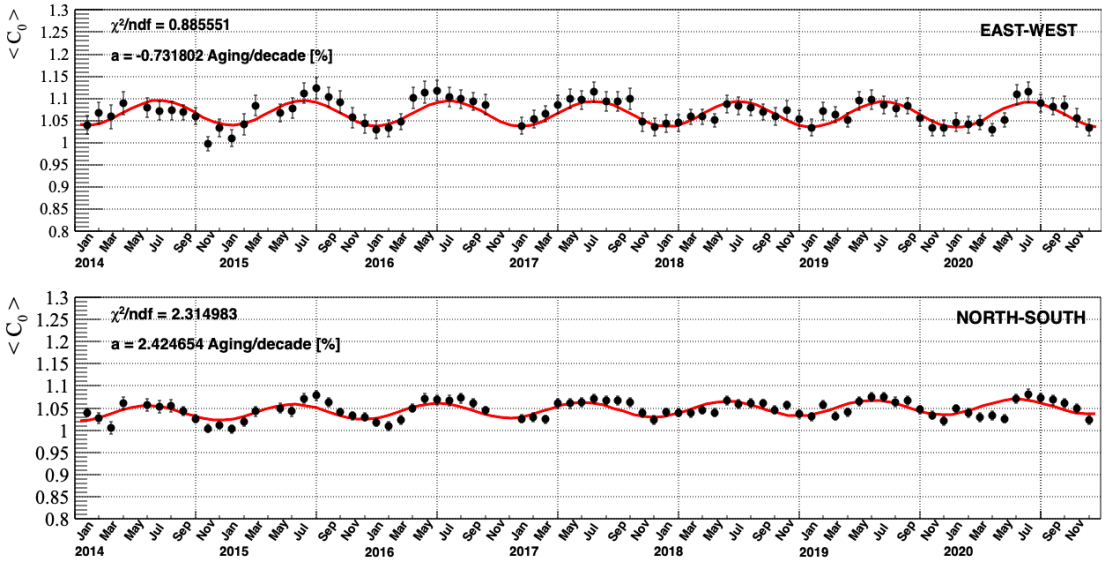

Figure 5: Calibration constants obtained for both channels of antenna Id:33 from 2014 to 2020. The corresponding cosine+linear fit is represented by the red curve.

This fit is done for all channels considered in this study. The distribution of the aging coefficients is shown in Fig.6. The estimation of aging, considering the different aging rates obtained for all antennas, is calculated as a weighted average, taking into account the uncertainties associated with each fit. Regarding the uncertainty estimation, it is worth mentioning that the fit does not describe the seasonal modulation perfectly. For instance, there are upward/downward fluctuations of the values of $\langle C_0 \rangle$ observed for all antennas at the same time in some specific periods. This reflects our lack of knowledge about the origin of the seasonal modulation and can potentially impact the resulting fitted aging coefficient, particularly in cases where significant fluctuations occur at the beginning or end of the data collection period. Therefore, we must be careful not to confuse actual aging with some effect that just happened to be higher in later/earlier years. To address this issue, we performed mock simulations of the calibration constants over time. In these mock simulations, for each antenna and month, we generate random Gaussian distributed values of calibration constants with mean and RMS equal to the measured $\langle C_0 \rangle$ value and its corresponding uncertainty. Then, we randomly shuffle the years for all antennas in a consistent manner and perform fits of the mocked calibration constants over time. The average of the mock agings coefficients should converge to zero, and the RMS of the mock aging distribution is our final estimate for the uncertainty in the aging parameter, taking into account strong fluctuations that occurred in specific periods unrelated to antenna aging. Considering this, we obtain an aging factor of $(0.3 \pm 1.4)\%$ and $(-0.1 \pm 1.1)\%$ per decade for East-West and North-South, respectively, for Butterfly stations. For LPDA antennas, which have a much smaller number of stations and a shorter period of data collection compared to Butterfly stations, we found an aging factor of $(-1.4 \pm 3.5)\%$ and $(-1.9 \pm 1.8)\%$ for the East-West and North-South channels, respectively. Combining all antenna types and channels, we obtain an

aging factor of $(-0.4 \pm 0.8)\%$ per decade. The results indicate that there is no significant or relevant aging effect observed in the AERA antennas.

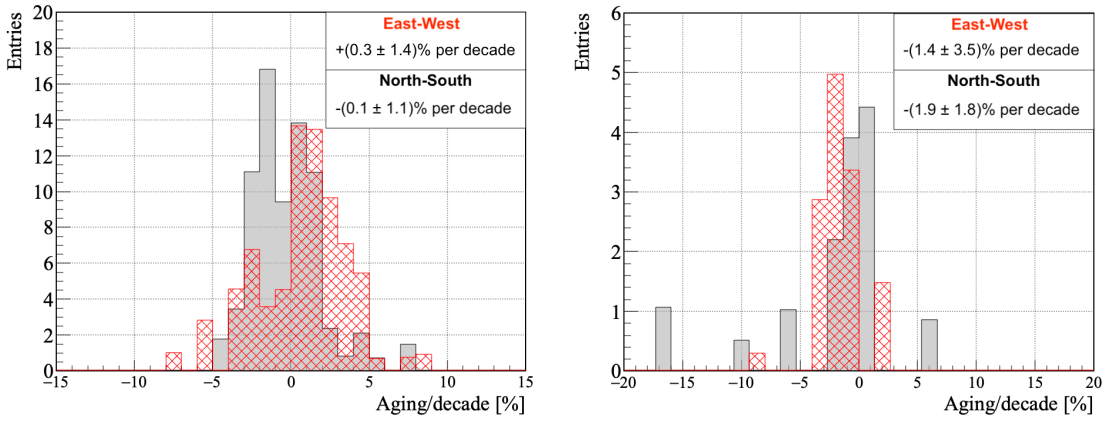

Figure 6: Distribution of the aging factor obtained for East-West (red histograms with hatch patterns) and North-South (solid gray histograms) channels. On the left, Butterfly stations. On the right, LPDA.

6. Conclusions

In this study, we conducted an absolute Galactic calibration of AERA stations, considering Butterfly and LPDA antennas. The calibration constants obtained were found to be close to unity, indicating a good agreement with the original calibration process, which involved laboratory measurements of the analogue chain and simulations to determine the directional response of the antenna. Additionally, we examined the behavior of the calibration constants over time for a period of almost a decade. The aging coefficients obtained from the fit of the evolution of the calibration constants as a function of time are very small and consistent with zero within uncertainties, indicating that there is no significant and no relevant aging effect observed in the AERA antennas.

This shows that radio detectors can effectively monitor aging effects in detectors operating over extended time periods. The results are particularly valuable in the context of the Pierre Auger Observatory upgrade [10] and the Radio Detector [11] and highlighting the importance of the radio detection technique for determining an absolute energy scale for cosmic rays.

References

[1] P.Abreu *et al.* [Pierre Auger coll.], JINST **7** (2012) P10011.
[2] E. Polisensky, Long Wavelength Array Memo Series **111** (2007) 515.
[3] de Oliveira-Costa, A., Tegmark, M., Gaensler, B. M., et al., MNRAS **388** (2008) 247–260.
[4] Dowell, J., Taylor, G. B., Schinzel, F. K., Kassim, et al., MNRAS **469** (2017) 4537–4550.
[5] Mayuri Sathyanarayana Rao, Ravi Subrahmanyan, et al., AJ **153** (2017) 26.
[6] Haslam, C. G. T., Salter, C. J., Stoffel, H., & Wilson, W. E, A&AS **47** (1982) 1.
[7] Yanping-Cong. Yanping-Cong/ULSA: (v2.0). Zenodo. https://doi.org/10.5281/zenodo.4663463 (2021).
[8] Büsken, T. Fodran and T. Huege, submitted to A&A, arXiv:2211.03086 (2022).
[9] K. Mulrey, A. Bonardi, S. Buitink, A. Corstanje, et al., Astropart. Phys. **111** (2019) 1-11.
[10] P.Abreu *et al.* [Pierre Auger coll.], arXiv:1604.03637 (2016).
[11] J. H. Hörandel *et al.* [Pierre Auger coll.], EPJ Web Conf. **210** (2019) 06005.

The Pierre Auger Collaboration

A. Abdul Halim[13], P. Abreu[72], M. Aglietta[54,52], I. Allekotte[1], K. Almeida Cheminant[70], A. Almela[7,12], R. Aloisio[45,46], J. Alvarez-Muñiz[79], J. Ammerman Yebra[79], G.A. Anastasi[54,52], L. Anchordoqui[86], B. Andrada[7], S. Andringa[72], C. Aramo[50], P.R. Araújo Ferreira[42], E. Arnone[63,52], J. C. Arteaga Velázquez[67], H. Asorey[7], P. Assis[72], G. Avila[11], E. Avocone[57,46], A.M. Badescu[75], A. Bakalova[32], A. Balaceanu[73], F. Barbato[45,46], A. Bartz Mocellin[85], J.A. Bellido[13,69], C. Berat[36], M.E. Bertaina[63,52], G. Bhatta[70], M. Bianciotto[63,52], P.L. Biermann[h], V. Binet[5], K. Bismark[39,7], T. Bister[80,81], J. Biteau[37], J. Blazek[32], C. Bleve[36], J. Blümer[41], M. Boháčová[32], D. Boncioli[57,46], C. Bonifazi[8,26], L. Bonneau Arbeletche[21], N. Borodai[70], J. Brack[j], P.G. Brichetto Orchera[7], F.L. Briechle[42], A. Bueno[78], S. Buitink[15], M. Buscemi[47,61], M. Büsken[39,7], A. Bwembya[80,81], K.S. Caballero-Mora[66], S. Cabana-Freire[79], L. Caccianiga[59,49], I. Caracas[38], R. Caruso[58,47], A. Castellina[54,52], F. Catalani[18], G. Cataldi[48], L. Cazon[79], M. Cerda[10], A. Cermenati[45,46], J.A. Chinellato[21], J. Chudoba[32], L. Chytka[33], R.W. Clay[13], A.C. Cobos Cerutti[6], R. Colalillo[60,50], A. Coleman[90], M.R. Coluccia[48], R. Conceição[72], A. Condorelli[37], G. Consolati[49,55], M. Conte[56,48], F. Convenga[41], D. Correia dos Santos[28], P.J. Costa[72], C.E. Covault[84], M. Cristinziani[44], C.S. Cruz Sanchez[3], S. Dasso[4,2], K. Daumiller[41], B.R. Dawson[13], R.M. de Almeida[28], J. de Jesús[7,41], S.J. de Jong[80,81], J.R.T. de Mello Neto[26,27], I. De Mitri[45,46], J. de Oliveira[17], D. de Oliveira Franco[21], F. de Palma[56,48], V. de Souza[19], E. De Vito[56,48], A. Del Popolo[58,47], O. Deligny[34], N. Denner[32], L. Deval[41,7], A. di Matteo[52], M. Dobre[73], C. Dobrigkeit[21], J.C. D'Olivo[68], L.M. Domingues Mendes[72], J.C. dos Anjos, R.C. dos Anjos[25], J. Ebr[32], F. Ellwanger[41], M. Emam[80,81], R. Engel[39,41], I. Epicoco[56,48], M. Erdmann[42], A. Etchegoyen[7,12], C. Evoli[45,46], H. Falcke[80,82,81], J. Farmer[89], G. Farrar[88], A.C. Fauth[21], N. Fazzini[e], F. Feldbusch[40], F. Fenu[41,d], A. Fernandes[72], B. Fick[87], J.M. Figueira[7], A. Filipčič[77,76], T. Fitoussi[41], B. Flaggs[90], T. Fodran[80], T. Fujii[89,f], A. Fuster[7,12], C. Galea[80], C. Galelli[59,49], B. García[6], C. Gaudu[38], H. Gemmeke[40], F. Gesualdi[7,41], A. Gherghel-Lascu[73], P.L. Ghia[34], U. Giaccari[48], M. Giammarchi[49], J. Glombitza[42,g], F. Gobbi[10], F. Gollan[7], G. Golup[1], M. Gómez Berisso[1], P.F. Gómez Vitale[11], J.P. Gongora[11], J.M. González[1], N. González[7], I. Goos[1], D. Góra[70], A. Gorgi[54,52], M. Gottowik[79], T.D. Grubb[13], F. Guarino[60,50], G.P. Guedes[22], E. Guido[44], S. Hahn[39], P. Hamal[32], M.R. Hampel[7], P. Hansen[3], D. Harari[1], V.M. Harvey[13], A. Haungs[41], T. Hebbeker[42], C. Hojvat[e], J.R. Hörandel[80,81], P. Horvath[33], M. Hrabovský[33], T. Huege[41,15], A. Insolia[58,47], P.G. Isar[74], P. Janecek[32], J.A. Johnsen[85], J. Jurysek[32], A. Kääpä[38], K.H. Kampert[38], B. Keilhauer[41], A. Khakurdikar[80], V.V. Kizakke Covilakam[7,41], H.O. Klages[41], M. Kleifges[40], F. Knapp[39], N. Kunka[40], B.L. Lago[16], N. Langner[42], M.A. Leigui de Oliveira[24], Y Lema-Capeans[79], V. Lenok[39], A. Letessier-Selvon[35], I. Lhenry-Yvon[34], D. Lo Presti[58,47], L. Lopes[72], L. Lu[91], Q. Luce[39], J.P. Lundquist[76], A. Machado Payeras[21], M. Majercakova[32], D. Mandat[32], B.C. Manning[13], P. Mantsch[e], S. Marafico[34], F.M. Mariani[59,49], A.G. Mariazzi[3], I.C. Mariş[14], G. Marsella[61,47], D. Martello[56,48], S. Martinelli[41,7], O. Martínez Bravo[64], M.A. Martins[79], M. Mastrodicasa[57,46], H.J. Mathes[41], J. Matthews[a], G. Matthiae[62,51], E. Mayotte[85,38], S. Mayotte[85], P.O. Mazur[e], G. Medina-Tanco[68], J. Meinert[38], D. Melo[7], A. Menshikov[40], C. Merx[41], S. Michal[33], M.I. Micheletti[5], L. Miramonti[59,49], S. Mollerach[1], F. Montanet[36], L. Morejon[38], C. Morello[54,52], A.L. Müller[32], K. Mulrey[80,81], R. Mussa[52], M. Muzio[88], W.M. Namasaka[38], S. Negi[32], L. Nellen[68], K. Nguyen[87], G. Nicora[9], M. Niculescu-Oglinzanu[73], M. Niechciol[44], D. Nitz[87], D. Nosek[31], V. Novotny[31], L. Nožka[33], A Nucita[56,48], L.A. Núñez[30], C. Oliveira[19], M. Palatka[32], J. Pallotta[9], S. Panja[32], G. Parente[79], T. Paulsen[38], J. Pawlowsky[38], M. Pech[32], J. Pękala[70], R. Pelayo[65], L.A.S. Pereira[23], E.E. Pereira Martins[39,7], J. Perez Armand[20], C. Pérez Bertolli[7,41], L. Perrone[56,48], S. Petrera[45,46], C. Petrucci[57,46], T. Pierog[41], M. Pimenta[72], M. Platino[7], B. Pont[80], M. Pothast[81,80], M. Pourmohammad Shahvar[61,47], P. Privitera[89], M. Prouza[32], A. Puyleart[87], S. Querchfeld[38], J. Rautenberg[38], D. Ravignani[7], M. Reininghaus[39], J. Ridky[32], F. Riehn[79], M. Risse[44], V. Rizi[57,46], W. Rodrigues de Carvalho[80], E. Rodriguez[7,41], J. Rodriguez Rojo[11], M.J. Roncoroni[7], S. Rossoni[43], M. Roth[41], E. Roulet[1], A.C. Rovero[4], P. Ruehl[44], A. Saftoiu[73], M. Saharan[80], F. Salamida[57,46], H. Salazar[64], G. Salina[51], J.D. Sanabria Gomez[30], F. Sánchez[7], E.M. Santos[20], E. Santos[32],

F. Sarazin[85], R. Sarmento[72], R. Sato[11], P. Savina[91], C.M. Schäfer[41], V. Scherini[56,48], H. Schieler[41], M. Schimassek[34], M. Schimp[38], F. Schlüter[41], D. Schmidt[39], O. Scholten[15,i], H. Schoorlemmer[80,81], P. Schovánek[32], F.G. Schröder[90,41], J. Schulte[42], T. Schulz[41], S.J. Sciutto[3], M. Scornavacche[7,41], A. Segreto[53,47], S. Sehgal[38], S.U. Shivashankara[76], G. Sigl[43], G. Silli[7], O. Sima[73,b], F. Simon[40], R. Smau[73], R. Šmída[89], P. Sommers[k], J.F. Soriano[86], R. Squartini[10], M. Stadelmaier[32], D. Stanca[73], S. Stanič[76], J. Stasielak[70], P. Stassi[36], S. Strähnz[39], M. Straub[42], M. Suárez-Durán[14], T. Suomijärvi[37], A.D. Supanitsky[7], Z. Svozilikova[32], Z. Szadkowski[71], A. Tapia[29], C. Taricco[63,52], C. Timmermans[81,80], O. Tkachenko[41], P. Tobiska[32], C.J. Todero Peixoto[18], B. Tomé[72], Z. Torrès[36], A. Travaini[10], P. Travnicek[32], C. Trimarelli[57,46], M. Tueros[3], M. Unger[41], L. Vaclavek[33], M. Vacula[33], J.F. Valdés Galicia[68], L. Valore[60,50], E. Varela[64], A. Vásquez-Ramírez[30], D. Veberič[41], C. Ventura[27], I.D. Vergara Quispe[3], V. Verzi[51], J. Vicha[32], J. Vink[83], J. Vlastimil[32], S. Vorobiov[76], C. Watanabe[26], A.A. Watson[c], A. Weindl[41], L. Wiencke[85], H. Wilczyński[70], D. Wittkowski[38], B. Wundheiler[7], B. Yue[38], A. Yushkov[32], O. Zapparrata[14], E. Zas[79], D. Zavrtanik[76,77], M. Zavrtanik[77,76]

———— • ————

[1] Centro Atómico Bariloche and Instituto Balseiro (CNEA-UNCuyo-CONICET), San Carlos de Bariloche, Argentina
[2] Departamento de Física and Departamento de Ciencias de la Atmósfera y los Océanos, FCEyN, Universidad de Buenos Aires and CONICET, Buenos Aires, Argentina
[3] IFLP, Universidad Nacional de La Plata and CONICET, La Plata, Argentina
[4] Instituto de Astronomía y Física del Espacio (IAFE, CONICET-UBA), Buenos Aires, Argentina
[5] Instituto de Física de Rosario (IFIR) – CONICET/U.N.R. and Facultad de Ciencias Bioquímicas y Farmacéuticas U.N.R., Rosario, Argentina
[6] Instituto de Tecnologías en Detección y Astropartículas (CNEA, CONICET, UNSAM), and Universidad Tecnológica Nacional – Facultad Regional Mendoza (CONICET/CNEA), Mendoza, Argentina
[7] Instituto de Tecnologías en Detección y Astropartículas (CNEA, CONICET, UNSAM), Buenos Aires, Argentina
[8] International Center of Advanced Studies and Instituto de Ciencias Físicas, ECyT-UNSAM and CONICET, Campus Miguelete – San Martín, Buenos Aires, Argentina
[9] Laboratorio Atmósfera – Departamento de Investigaciones en Láseres y sus Aplicaciones – UNIDEF (CITEDEF-CONICET), Argentina
[10] Observatorio Pierre Auger, Malargüe, Argentina
[11] Observatorio Pierre Auger and Comisión Nacional de Energía Atómica, Malargüe, Argentina
[12] Universidad Tecnológica Nacional – Facultad Regional Buenos Aires, Buenos Aires, Argentina
[13] University of Adelaide, Adelaide, S.A., Australia
[14] Université Libre de Bruxelles (ULB), Brussels, Belgium
[15] Vrije Universiteit Brussels, Brussels, Belgium
[16] Centro Federal de Educação Tecnológica Celso Suckow da Fonseca, Petropolis, Brazil
[17] Instituto Federal de Educação, Ciência e Tecnologia do Rio de Janeiro (IFRJ), Brazil
[18] Universidade de São Paulo, Escola de Engenharia de Lorena, Lorena, SP, Brazil
[19] Universidade de São Paulo, Instituto de Física de São Carlos, São Carlos, SP, Brazil
[20] Universidade de São Paulo, Instituto de Física, São Paulo, SP, Brazil
[21] Universidade Estadual de Campinas, IFGW, Campinas, SP, Brazil
[22] Universidade Estadual de Feira de Santana, Feira de Santana, Brazil
[23] Universidade Federal de Campina Grande, Centro de Ciencias e Tecnologia, Campina Grande, Brazil
[24] Universidade Federal do ABC, Santo André, SP, Brazil
[25] Universidade Federal do Paraná, Setor Palotina, Palotina, Brazil
[26] Universidade Federal do Rio de Janeiro, Instituto de Física, Rio de Janeiro, RJ, Brazil
[27] Universidade Federal do Rio de Janeiro (UFRJ), Observatório do Valongo, Rio de Janeiro, RJ, Brazil
[28] Universidade Federal Fluminense, EEIMVR, Volta Redonda, RJ, Brazil
[29] Universidad de Medellín, Medellín, Colombia
[30] Universidad Industrial de Santander, Bucaramanga, Colombia

[31] Charles University, Faculty of Mathematics and Physics, Institute of Particle and Nuclear Physics, Prague, Czech Republic
[32] Institute of Physics of the Czech Academy of Sciences, Prague, Czech Republic
[33] Palacky University, Olomouc, Czech Republic
[34] CNRS/IN2P3, IJCLab, Université Paris-Saclay, Orsay, France
[35] Laboratoire de Physique Nucléaire et de Hautes Energies (LPNHE), Sorbonne Université, Université de Paris, CNRS-IN2P3, Paris, France
[36] Univ. Grenoble Alpes, CNRS, Grenoble Institute of Engineering Univ. Grenoble Alpes, LPSC-IN2P3, 38000 Grenoble, France
[37] Université Paris-Saclay, CNRS/IN2P3, IJCLab, Orsay, France
[38] Bergische Universität Wuppertal, Department of Physics, Wuppertal, Germany
[39] Karlsruhe Institute of Technology (KIT), Institute for Experimental Particle Physics, Karlsruhe, Germany
[40] Karlsruhe Institute of Technology (KIT), Institut für Prozessdatenverarbeitung und Elektronik, Karlsruhe, Germany
[41] Karlsruhe Institute of Technology (KIT), Institute for Astroparticle Physics, Karlsruhe, Germany
[42] RWTH Aachen University, III. Physikalisches Institut A, Aachen, Germany
[43] Universität Hamburg, II. Institut für Theoretische Physik, Hamburg, Germany
[44] Universität Siegen, Department Physik – Experimentelle Teilchenphysik, Siegen, Germany
[45] Gran Sasso Science Institute, L'Aquila, Italy
[46] INFN Laboratori Nazionali del Gran Sasso, Assergi (L'Aquila), Italy
[47] INFN, Sezione di Catania, Catania, Italy
[48] INFN, Sezione di Lecce, Lecce, Italy
[49] INFN, Sezione di Milano, Milano, Italy
[50] INFN, Sezione di Napoli, Napoli, Italy
[51] INFN, Sezione di Roma "Tor Vergata", Roma, Italy
[52] INFN, Sezione di Torino, Torino, Italy
[53] Istituto di Astrofisica Spaziale e Fisica Cosmica di Palermo (INAF), Palermo, Italy
[54] Osservatorio Astrofisico di Torino (INAF), Torino, Italy
[55] Politecnico di Milano, Dipartimento di Scienze e Tecnologie Aerospaziali , Milano, Italy
[56] Università del Salento, Dipartimento di Matematica e Fisica "E. De Giorgi", Lecce, Italy
[57] Università dell'Aquila, Dipartimento di Scienze Fisiche e Chimiche, L'Aquila, Italy
[58] Università di Catania, Dipartimento di Fisica e Astronomia "Ettore Majorana", Catania, Italy
[59] Università di Milano, Dipartimento di Fisica, Milano, Italy
[60] Università di Napoli "Federico II", Dipartimento di Fisica "Ettore Pancini", Napoli, Italy
[61] Università di Palermo, Dipartimento di Fisica e Chimica "E. Segrè", Palermo, Italy
[62] Università di Roma "Tor Vergata", Dipartimento di Fisica, Roma, Italy
[63] Università Torino, Dipartimento di Fisica, Torino, Italy
[64] Benemérita Universidad Autónoma de Puebla, Puebla, México
[65] Unidad Profesional Interdisciplinaria en Ingeniería y Tecnologías Avanzadas del Instituto Politécnico Nacional (UPIITA-IPN), México, D.F., México
[66] Universidad Autónoma de Chiapas, Tuxtla Gutiérrez, Chiapas, México
[67] Universidad Michoacana de San Nicolás de Hidalgo, Morelia, Michoacán, México
[68] Universidad Nacional Autónoma de México, México, D.F., México
[69] Universidad Nacional de San Agustin de Arequipa, Facultad de Ciencias Naturales y Formales, Arequipa, Peru
[70] Institute of Nuclear Physics PAN, Krakow, Poland
[71] University of Łódź, Faculty of High-Energy Astrophysics,Łódź, Poland
[72] Laboratório de Instrumentação e Física Experimental de Partículas – LIP and Instituto Superior Técnico – IST, Universidade de Lisboa – UL, Lisboa, Portugal
[73] "Horia Hulubei" National Institute for Physics and Nuclear Engineering, Bucharest-Magurele, Romania
[74] Institute of Space Science, Bucharest-Magurele, Romania
[75] University Politehnica of Bucharest, Bucharest, Romania
[76] Center for Astrophysics and Cosmology (CAC), University of Nova Gorica, Nova Gorica, Slovenia
[77] Experimental Particle Physics Department, J. Stefan Institute, Ljubljana, Slovenia

PoS(ICRC2023)279

[78] Universidad de Granada and C.A.F.P.E., Granada, Spain
[79] Instituto Galego de Física de Altas Enerxías (IGFAE), Universidade de Santiago de Compostela, Santiago de Compostela, Spain
[80] IMAPP, Radboud University Nijmegen, Nijmegen, The Netherlands
[81] Nationaal Instituut voor Kernfysica en Hoge Energie Fysica (NIKHEF), Science Park, Amsterdam, The Netherlands
[82] Stichting Astronomisch Onderzoek in Nederland (ASTRON), Dwingeloo, The Netherlands
[83] Universiteit van Amsterdam, Faculty of Science, Amsterdam, The Netherlands
[84] Case Western Reserve University, Cleveland, OH, USA
[85] Colorado School of Mines, Golden, CO, USA
[86] Department of Physics and Astronomy, Lehman College, City University of New York, Bronx, NY, USA
[87] Michigan Technological University, Houghton, MI, USA
[88] New York University, New York, NY, USA
[89] University of Chicago, Enrico Fermi Institute, Chicago, IL, USA
[90] University of Delaware, Department of Physics and Astronomy, Bartol Research Institute, Newark, DE, USA
[91] University of Wisconsin-Madison, Department of Physics and WIPAC, Madison, WI, USA

—

[a] Louisiana State University, Baton Rouge, LA, USA
[b] also at University of Bucharest, Physics Department, Bucharest, Romania
[c] School of Physics and Astronomy, University of Leeds, Leeds, United Kingdom
[d] now at Agenzia Spaziale Italiana (ASI). Via del Politecnico 00133, Roma, Italy
[e] Fermi National Accelerator Laboratory, Fermilab, Batavia, IL, USA
[f] now at Graduate School of Science, Osaka Metropolitan University, Osaka, Japan
[g] now at ECAP, Erlangen, Germany
[h] Max-Planck-Institut für Radioastronomie, Bonn, Germany
[i] also at Kapteyn Institute, University of Groningen, Groningen, The Netherlands
[j] Colorado State University, Fort Collins, CO, USA
[k] Pennsylvania State University, University Park, PA, USA

Acknowledgments

The successful installation, commissioning, and operation of the Pierre Auger Observatory would not have been possible without the strong commitment and effort from the technical and administrative staff in Malargüe. We are very grateful to the following agencies and organizations for financial support:

Argentina – Comisión Nacional de Energía Atómica; Agencia Nacional de Promoción Científica y Tecnológica (ANPCyT); Consejo Nacional de Investigaciones Científicas y Técnicas (CONICET); Gobierno de la Provincia de Mendoza; Municipalidad de Malargüe; NDM Holdings and Valle Las Leñas; in gratitude for their continuing cooperation over land access; Australia – the Australian Research Council; Belgium – Fonds de la Recherche Scientifique (FNRS); Research Foundation Flanders (FWO); Brazil – Conselho Nacional de Desenvolvimento Científico e Tecnológico (CNPq); Financiadora de Estudos e Projetos (FINEP); Fundação de Amparo à Pesquisa do Estado de Rio de Janeiro (FAPERJ); São Paulo Research Foundation (FAPESP) Grants No. 2019/10151-2, No. 2010/07359-6 and No. 1999/05404-3; Ministério da Ciência, Tecnologia, Inovações e Comunicações (MCTIC); Czech Republic – Grant No. MSMT CR LTT18004, LM2015038, LM2018102, CZ.02.1.01/0.0/0.0/16_013/0001402, CZ.02.1.01/0.0/0.0/18_046/0016010 and CZ.02.1.01/0.0/0.0/17_049/0008422; France – Centre de Calcul IN2P3/CNRS; Centre National de la Recherche Scientifique (CNRS); Conseil Régional Ile-de-France; Département Physique Nucléaire et Corpusculaire (PNC-IN2P3/CNRS); Département Sciences de l'Univers (SDU-INSU/CNRS); Institut Lagrange de Paris (ILP) Grant No. LABEX ANR-10-LABX-63 within the Investissements d'Avenir Programme Grant No. ANR-11-IDEX-0004-02; Germany – Bundesministerium für Bildung und Forschung (BMBF); Deutsche Forschungsgemeinschaft (DFG); Finanzministerium Baden-Württemberg; Helmholtz Alliance for Astroparticle Physics (HAP); Helmholtz-Gemeinschaft Deutscher Forschungszentren (HGF); Ministerium für Kultur und Wissenschaft des Landes Nordrhein-Westfalen; Ministerium für Wissenschaft, Forschung und Kunst des Landes Baden-Württemberg; Italy – Istituto Nazionale di Fisica Nucleare (INFN); Istituto Nazionale di Astrofisica (INAF); Ministero dell'Universitá e della Ricerca (MUR); CETEMPS Center of Excellence; Ministero degli Affari Esteri (MAE), ICSC Centro Nazionale di Ricerca in High Performance Computing, Big Data

and Quantum Computing, funded by European Union NextGenerationEU, reference code CN_00000013; México – Consejo Nacional de Ciencia y Tecnología (CONACYT) No. 167733; Universidad Nacional Autónoma de México (UNAM); PAPIIT DGAPA-UNAM; The Netherlands – Ministry of Education, Culture and Science; Netherlands Organisation for Scientific Research (NWO); Dutch national e-infrastructure with the support of SURF Cooperative; Poland – Ministry of Education and Science, grants No. DIR/WK/2018/11 and 2022/WK/12; National Science Centre, grants No. 2016/22/M/ST9/00198, 2016/23/B/ST9/01635, 2020/39/B/ST9/01398, and 2022/45/B/ST9/02163; Portugal – Portuguese national funds and FEDER funds within Programa Operacional Factores de Competitividade through Fundação para a Ciência e a Tecnologia (COMPETE); Romania – Ministry of Research, Innovation and Digitization, CNCS-UEFISCDI, contract no. 30N/2023 under Romanian National Core Program LAPLAS VII, grant no. PN 23 21 01 02 and project number PN-III-P1-1.1-TE-2021-0924/TE57/2022, within PNCDI III; Slovenia – Slovenian Research Agency, grants P1-0031, P1-0385, I0-0033, N1-0111; Spain – Ministerio de Economía, Industria y Competitividad (FPA2017-85114-P and PID2019-104676GB-C32), Xunta de Galicia (ED431C 2017/07), Junta de Andalucía (SOMM17/6104/UGR, P18-FR-4314) Feder Funds, RENATA Red Nacional Temática de Astropartículas (FPA2015-68783-REDT) and María de Maeztu Unit of Excellence (MDM-2016-0692); USA – Department of Energy, Contracts No. DE-AC02-07CH11359, No. DE-FR02-04ER41300, No. DE-FG02-99ER41107 and No. DE-SC0011689; National Science Foundation, Grant No. 0450696; The Grainger Foundation; Marie Curie-IRSES/EPLANET; European Particle Physics Latin American Network; and UNESCO.